BIOCHEMISTRY
including biophysical chemistry & molecular biology

Article

pubs.acs.org/biochemistry

Effects of Protein Structure on Iron–Polypeptide Vibrational Dynamic Coupling in Cytochrome *c*

Mary Grace I. Galinato,*[,†,‡] Sarah E. J. Bowman,[§] Jesse G. Kleingardner,[§] Sherri Martin,[†] Jiyong Zhao,[∥] Wolfgang Sturhahn,[∥] E. Ercan Alp,[∥] Kara L. Bren,*[,§] and Nicolai Lehnert*[,†]

[†]Department of Chemistry, University of Michigan, Ann Arbor, Michigan 48109, United States

[‡]School of Science-Chemistry, Penn State Erie, The Behrend College, Erie, Pennsylvania 16563, United States

[§]Department of Chemistry, University of Rochester, Rochester, New York 14627, United States

[∥]Advanced Photon Source/Experimental Facilities Division, Argonne National Laboratory, Argonne, Illinois 60439, United States

Supporting Information

ABSTRACT: Cytochrome *c* (Cyt *c*) has a heme covalently bound to the polypeptide via a Cys-X-X-Cys-His (CXXCH) linker that is located in the interface region for protein–protein interactions. To determine whether the polypeptide matrix influences iron vibrational dynamics, nuclear resonance vibrational spectroscopy (NRVS) measurements were performed on ^{57}Fe-labeled ferric *Hydrogenobacter thermophilus* cytochrome *c*-552, and variants M13V, M13V/K22M, and A7F, which have structural modifications that alter the composition or environment of the CXXCH pentapeptide loop. Simulations of the NRVS data indicate that the 150–325 cm^{-1} region is dominated by N_{His}–Fe–S_{Met} axial ligand and polypeptide motions, while the 325–400 cm^{-1} region shows dominant contributions from ν(Fe–N_{Pyr}) (Pyr = pyrrole) and other heme-based modes. Diagnostic spectral signatures that directly relate to structural features of the heme active site are identified using a quantum chemistry-centered normal coordinate analysis (QCC-NCA). In particular, spectral features that directly correlate with CXXCH loop stiffness, the strength of the Fe–His interaction, and the degree of heme distortion are identified. Cumulative results from our investigation suggest that compared to the wild type (wt), variants M13V and M13V/K22M have a more rigid CXXCH pentapeptide segment, a stronger Fe–N_{His} interaction, and a more ruffled heme. Conversely, the A7F variant has a more planar heme and a weaker Fe–N_{His} bond. These results are correlated to the observed changes in reduction potential between wt protein and the variants studied here. Implications of these results for Cyt *c* biogenesis and electron transfer are also discussed.

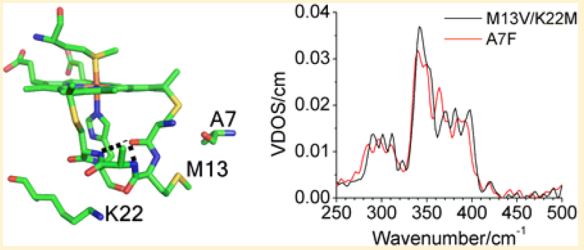

Biological function requires protein conformational dynamics on a wide range of time scales. There is an ever-increasing body of evidence that fast (subnanosecond) dynamics of proteins, including vibrations, are functionally important.[1] Experimental studies of polypeptide vibrational dynamics are challenging because of the large number of vibrational modes of similar energies. Nevertheless, analysis of polypeptide infrared[2] or UV resonance Raman spectra[3] yields information about overall protein vibrational dynamics. To obtain site-specific information about dynamics, a chromophore with resolved or enhanced vibrational modes is needed. For example, aromatic amino acids or metal ions may show enhancement in resonance Raman spectra,[3−5] and the introduction of C–D bonds yields resolved vibrational bands for the C–H(D) stretching modes.[6] In another approach, two-dimensional IR spectroscopy of small complexes bound to proteins has provided detailed information about protein dynamics sensed by the complex.[7,8] The approach taken herein is to employ nuclear resonance vibrational spectroscopy (NRVS), in which vibrations of a Mössbauer-active nucleus are detected (here, ^{57}Fe).[9] NRVS offers a significant advantage in that its selection rules allow detection of *all* motions involving ^{57}Fe, with intensities scaling with the amount of ^{57}Fe motion in a given mode, facilitating detailed analysis and interpretation of spectral data.[10−15]

The NRVS data of ^{57}Fe within a metal complex depend critically on the vibrations of its ligands, and thus, NRVS reveals key information about metal–ligand bonding and dynamics.[13,16] Furthermore, within a metalloprotein, the probe nucleus vibrations are also coupled to those of the surrounding polypeptide. This ^{57}Fe–polypeptide coupling was recently demonstrated in a NRVS study on the ferric heme protein *Hydrogenobacter thermophilus* cytochrome *c*-552 (*Ht c*-552) with the help of isotopic labeling of the porphyrin, the polypeptide, and specific amino acid residues. In particular, the heme iron in *Ht c*-552 was found to be strongly vibrationally coupled to amino acid residues on the protein surface that are expected to interact with redox partners.[17] This result suggests

Received: November 19, 2014
Revised: December 19, 2014
Published: December 22, 2014

DOI: 10.1021/bi501430z
Biochemistry 2015, 54, 1064−1076

that protein−protein interactions may influence iron dynamics and electron transfer (ET) rates.

To test the hypothesis that the polypeptide matrix influences iron vibrational dynamics in cytochromes *c*, here we analyze ^{57}Fe NRVS data on a series of mutants of *Ht c*-552 (Figure 1). *Ht c*-552 is a member of the well-studied group of class I monoheme cytochromes *c* that play key roles in respiration, photosynthesis, and apoptosis.[18−20] Cytochromes *c* are distinguished from other heme-containing proteins by the covalent bonding between the porphyrin and the polypeptide. The heme is usually attached to a Cys-X-X-Cys-His (CXXCH) motif in which the X's are variable residues, the Cys residues form thioether bonds to two porphyrin substituents, and the His coordinates the heme iron (Figure 1).[18] For *Ht c*-552, "XX" in the CXXCH segment represents Met13 and Ala14. The mutants chosen alter the composition or environment of the CXXCH motif and, in this way, have been shown to affect the reduction potential of the heme. The A7F mutant is proposed to decrease the level of hydrogen bonding between the backbone atoms of residue 7 and Cys12, the first residue of the CXXCH motif. Previous studies of this mutant indicate that this subtle change causes a small decrease in the amount of out-of-plane heme distortion known as ruffling [in which the Fe−N(pyrrole) bonds are twisted in alternate directions (Figure S1 of the Supporting Information)] and a small *increase* in the heme reduction potential.[21] The M13V mutation of the first variable residue within the CXXCH segment has been shown to increase the level of heme ruffling, *decrease* the reduction potential, and increase the strength of the Fe(III)−His bond; these effects are proposed to result from improved packing of hydrophobic residues interacting with the CXXCH peptide. Finally, the M13V/K22M double mutant further enhances packing beyond what is accomplished by the M13V mutation via replacement of the polar Lys22 with the hydrophobic Met, which is then proposed to pack against Val13 within the CXXCH motif. This double mutant shows a yet higher level of heme ruffling, a lower reduction potential, and a strengthened Fe(III)−His bond relative to those of M13V.[22−24] Furthermore, NMR studies of M13V and M13V/K22M have shown that the CXXCH peptide is rigidified by these mutations as revealed by hydrogen exchange.[22] This well-characterized series of mutants presents an excellent set of subjects for elucidating the relationship between interactions with(in) the CXXCH motif and iron vibrational dynamics, and how this affects ET.

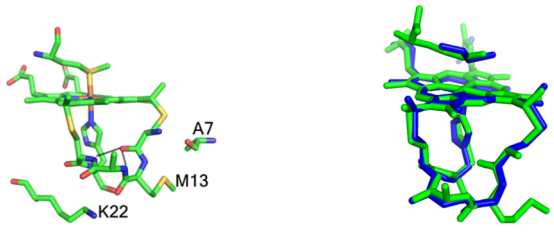

Figure 1. Active site structure (left) of *Ht c*-552 (Protein Data Bank entry 1YNR), highlighting amino acid residues targeted in this study. The black lines represent key H-bonding interactions between the N−H groups of Cys15 and His16 and the C═O group of Cys 12. Overlay (right) of the model (blue) and crystal structure of *Ht c*-552 (green). In generating the model, residues 7 and 22 were not included. Instead, the changes affected by mutating residues 7, 13, and 22 were simulated in the NRVS analysis (see the text).

EXPERIMENTAL PROCEDURES

Expression and Purification of Protein Samples. *H. thermophilus* cytochrome *c*-552 (*Ht c*-552) and its A7F,[21] M13V,[22] and M13V/K22M[22] mutants were expressed in *Escherichia coli* strain BL21(DE3) and purified using methods described previously for wild-type (wt) *Ht c*-552.[17] Samples for NRVS data collection were enriched with ^{57}Fe by expression in modified minimal growth medium[21] supplemented with $^{57}FeSO_4 \cdot 1.2H_2O$ (20 mg/L) prepared from ^{57}Fe metal (Cambridge Isotope Laboratories) and 40% H_2SO_4. Purified protein was exchanged into 10 mM ammonium acetate buffer (pH 7) and lyophilized.

Resonance Raman Spectroscopy. Resonance Raman spectra of 0.2 mL of ∼300 μM solutions of wt *Ht c*-552 and M13V/K22M were recorded by selective excitation (413 and 514 nm, 20 mW) using a SpectraPhysics Beamlock 2060-RS Ar/Kr ion gas laser. The excitation beam was focused on the sample in an EPR coldfinger Dewar with liquid N_2 to prevent thermal degradation. The photons scattered from the sample were dispersed by an Acton two-stage TriVista 555 monochromator and focused on a N_2(l)-cooled Spec-10:400B/LN CCD camera (Princeton Instruments). The spectral resolution was set to 0.5 cm^{-1}, and the spectra were recorded with a 5 min accumulation time.

Nuclear Resonance Vibrational Spectroscopy. Samples for NRVS consisted of freshly prepared (within 1 month of data collection) lyophilized protein samples. Immediately before data collection, lyophilized ^{57}Fe-labeled protein was dissolved in 50 mM HEPES buffer (pH 7) containing 10% (v/v) glycerol to yield protein concentrations of 16−18 mM. To prevent reduction of heme during data collection, 4 μL of a saturated solution of K_2IrCl_6 was added to each NRVS sample (total volume of 60−70 μL). Samples were loaded into acrylic NRVS cells and frozen in N_2(l) for data collection. NRVS was performed on beamline 3-ID-XOR at the Advanced Photon Source of Argonne National Laboratory (Argonne, IL). A single NRVS scan required approximately 40 min and was performed in the range of −50 meV (−403.3 cm^{-1}) to +65 meV (524.3 cm^{-1}) for $E - E_0$ [the energy difference between the vibrational side bands detected and the central resonance due to the recoil-less excitation of the ^{57}Fe nuclear excited state (the Mössbauer transition)]. The resolution of the NRVS data is 8 cm^{-1}; the accuracy, on the other hand, is higher (approximately 1−2 cm^{-1}), because the data are calibrated to the intense, elastic scattering band corresponding to the Mössbauer line. Details of the other relevant parameters are given in ref 14. Depending on the protein sample, 15−18 scans were performed to achieve an acceptable signal-to-noise ratio (Table S1 of the Supporting Information).

DFT Model of *Ht c*-552. The active site model was based on a high-resolution crystal structure of *Ht c*-552 [Protein Data Bank (PDB) entry 1YNR]. The model consists of heme *c*, the distal Met side chain, the covalently linked CMACH segment (residues 12−16) with the Met13 and Ala14 residues truncated at the α-carbons, and formaldehyde in place of the Pro25 backbone carbonyl, which forms a H-bond to the His16 HNδ^1. All atoms were initially optimized using the BP86 functional[25,26] and LanL2DZ* basis set,[14,27−29] as implemented in Gaussian 03. After the structure had been optimized, the peptide segment (CMACH linker arm) was slightly adjusted to better resemble the crystal structure of the pentapeptide loop. The linker arm was then reoptimized using the same functional

DOI: 10.1021/bi501430z
Biochemistry 2015, 54, 1064−1076

and basis set while the coordinates of the heme, the Met side chain, the His ring, and formaldehyde and the two H-bonding distances (Cys15 NH to Cys12 CO and His16 NH to Cys12 CO) were fixed. This was done to more accurately reproduce the structure of the pentapeptide segment in the crystal structure (Figure 1, right) and, therefore, obtain a better description of the DFT-calculated NRVS data of Fe(III) *Ht c*-552. Vibrational frequencies were calculated for the final optimized structure using the BP86/LanL2DZ* level of theory.

QCC-NCA NRVS Simulation. The NRVS spectra of wt *Ht c*-552 and the variants (M13V, M13V/K22M, and A7F) were simulated using the Quantum-Chemistry Centered Normal Coordinate Analysis (QCC-NCA) package.[30,31] To describe the *Ht c*-552 active site model applied here (see Figure 1), 524 internal coordinates and 137550 (diagonal and off-diagonal) force constants are required. Of these force constants, ∼180 parameters were adjusted (within reason) to simulate the experimental data. The experimental spectra of the $^{13}C^{15}N$ polypeptide (pp)-, $^{13}C_5{}^{15}N$ Met-, and $^{13}C_8$ heme-labeled Fe(III) *Ht c*-552 samples[17] were used as a guide in adjusting the DFT-generated force constants to simulate the experimental wt NRVS data and the spectra of the isotopically-labeled proteins. For variants M13V and M13V/K22M, the force constants corresponding to the following coordinates were adjusted: the H-bonds in the pentapeptide segment (Cys15 NH to Cys12 CO and His16 NH to Cys12 CO), the CXXCH linker arm, and the Fe−N_{His} bond. In both cases, the H-bonds and the Fe−N_{His} bond were strengthened, and the CXXCH loop was made more rigid. These changes are based on the proposed modifications produced from these point mutations (see below for more details). To test the effect of heme distortion, the heme coordinates were first adjusted in GaussView 5.0. The degree of out-of-plane (oop) heme distortion in the model was then verified using Normal-Coordinate Structural Decomposition (NSD version 3.0) (Sandia National Laboratories). The two models that were constructed involve "more-ruffled" and "less-ruffled" forms of the heme (Figure S1 and Table S2 of the Supporting Information). In the former, the model displays a more prominent ruffling distortion (−1.0 Å) compared to the heme distortion in the wt protein model (−0.78 Å) to mimic the effects of the M13V and M13V/K22M mutations on the heme conformation. The change in the amount of ruffling was imposed while retaining the modified force constants mentioned above. The less-ruffled model was used to mimic the extent of heme ruffling in the A7F variant. Here, the heme coordinates were adjusted such that the level of heme ruffling decreases (to −0.65 Å). It is noted that the heme in *Pseudomonas aeruginosa* Cyt *c* (−0.48 Å) can be used to roughly mimic *Ht* A7F. In the simulation of the NRVS data of A7F, only very minor adjustments (<5%) were made to the force constants of the N_{His}−Fe−S_{Met} axial unit, the heme, and the linker arm.

The theoretical frequencies generated through QCC-NCA for ferric wt *Ht c*-552 are listed in the 165−500 cm^{-1} region in Table S4 of the Supporting Information. However, the experimental data cannot be reliably assigned in the energy region below 270 cm^{-1}, because the intensities of these features are too weak experimentally.

RESULTS AND ANALYSIS

Resonance Raman Spectra of Ferric *Ht c*-552 and Its Variants. Resonance Raman spectroscopy is a valuable tool that can selectively probe the vibrations of a chromophore within a protein matrix.[32−34] In general, the resonance Raman spectra of metalloporphyrins are sensitive to the oxidation and spin state, and the coordination number of the central metal.[33−36] Curiously, however, in the case of Cyt *c*, it has been observed that the low-energy region of the resonance Raman spectra (200−500 cm^{-1} range) is insensitive to the oxidation state of the metal. Here, the ferrous and ferric forms of the protein deliver essentially identical spectra in this region upon Soret excitation.[37] For ferric wt *Ht c*-552, prominent resonance Raman peaks in the 200−500 cm^{-1} region occur at 350, 357, 382, 400, 421, and 427 cm^{-1} as shown in Figure S2 of the Supporting Information. We then explored how the resonance Raman spectrum of this protein changes in the M13V/K22M double mutant (see below for further information about this variant). Figure S2 of the Supporting Information shows a direct comparison of the Soret-enhanced resonance Raman spectra of *Ht c*-552 and M13V/K22M, which does not reveal any spectral band shifts. In this energy region, the much-debated ν(Fe−N_{His}) and ν(Fe−S_{Met}) stretching modes occur, both of which have recently been assigned for *Ht c*-552 by our groups.[17] Our resonance Raman results suggest that the Raman-active Fe-ligand and porphyrin-based vibrations in the low-energy spectral region are insensitive to the differences between wt protein and the double mutant investigated here, analogous to their insensitivity to the iron oxidation state. Instead, nuclear resonance vibrational spectroscopy (NRVS) turned out to be much more suitable for investigating subtle differences between *Ht c*-552 and our active site mutants. Similarly, Sage and co-workers found that NRVS showed distinct differences in the vibrational spectra for ferrous and ferric horse heart Cyt *c* that were not seen by resonance Raman.[37]

NRVS Spectra of *Ht c*-552 Variants. The site-directed mutants M13V, M13V/K22M, and A7F (see Figure 1, left) have previously been investigated to determine the structural basis for the fine-tuning of the heme reduction potential in Cyt *c*.[22] The work presented here extends the prior studies by linking changes in the NRVS spectra of the *Ht c*-552 variants to structural modifications induced by specific point mutation(s). As recently established by us, the heme active site and the protein matrix in Cyt *c* are strongly vibrationally coupled, as evidenced by NRVS data of *Ht c*-552.[17] *This observation means that the heme vibrations should be sensitive to geometric changes in the proximity of heme, in particular in and near the CXXCH loop that is covalently linked to heme.* As shown in this study, this is in fact the case, but because of the complex NRVS data of *Ht c*-552 and its mutants, QCC-NCA is required to appropriately analyze the observed spectral changes.

The NRVS data of ferric *Ht c*-552 shown in the top panel of Figure 2 have previously been reported.[17] These data show intense features (corresponding to the modes with the largest iron displacement) in the 325−400 cm^{-1} region, which have been resolved into seven distinct peaks via Gaussian deconvolution (Figure 2 and Figure S3 of the Supporting Information). At lower energy, a weaker three-band spectral feature, observed in the 250−325 cm^{-1} region, is resolved into five Gaussian bands. The NRVS data of *Ht c*-552 have previously been assigned as reported in detail in ref 17. Any structural modifications to the protein matrix in the heme pocket will influence the vibrational motions of the heme and, hence, lead to perturbations of the NRVS data.

DOI: 10.1021/bi501430z
Biochemistry 2015, 54, 1064−1076

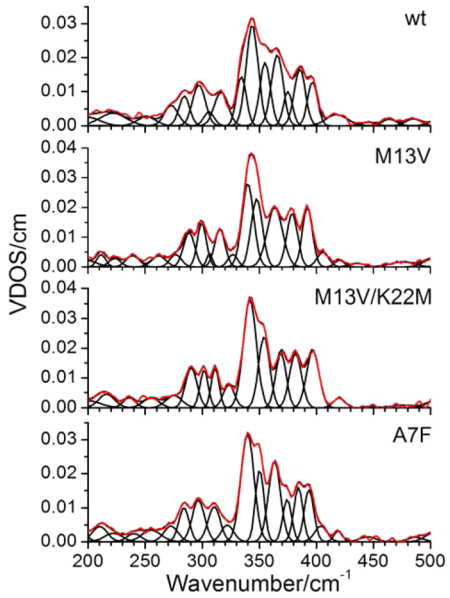

Figure 2. NRVS data of ferric wt *Ht c*-552 (taken from ref 17) and variants M13V, M13V/K22M, and A7F (red traces). Gaussian fits of these data are included (black traces).

Central among the *Ht c*-552 variants investigated in this work are those that perturb the conformational flexibility of the CXXCH polypeptide loop, which links the heme *c* prosthetic group to the protein matrix via two Cys residues. Importantly, two H-bonds exist between the N−H groups of Cys15 and His16 and the C═O group of Cys12 (Figure 1, left).[38] These hydrogen bonds span the CXXCH loop and potentially help stabilize the loop motif. These noncovalent interactions are influenced by the specific mutations incorporated into the set of *Ht c*-552 variants examined in this work. The H-bonding within the loop is also proposed to influence the Fe−N_{His} coordination and the degree of heme distortion, which are discussed below.

In the first variant that we investigated, M13V, the CXXCH pentapeptide is more rigid than in wt. This conclusion is based on hydrogen exchange studies that probe the energetics of the pentapeptide conformational fluctuations, which in turn affect heme−ligand interactions and heme reduction potential.[22] The enhanced H-bonding interactions across the loop in M13V are associated with a stronger Fe−N_{His} interaction and an increased degree of heme ruffling. These changes have been observed spectroscopically and are also accompanied by a lowering of the heme reduction potential of the single mutant (177 mV vs SHE) relative to that of wt (236 mV).[22] The structural modifications in M13V are reflected by a NRVS spectrum that exhibits key differences compared to that of wt as shown in Figure 2. In the low-energy region (275−325 cm^{-1}), the weak three-band spectral feature is resolved into five distinct Gaussian bands. Compared to wt, the overall spectral features in this region are retained; however, the NRVS intensities in the variant between 275 and 325 cm^{-1} are increased by approximately one-third compared to those of wt (also see Figure 6). In addition, the two bands found at 289 and 299 cm^{-1} in M13V are shifted to higher energy by approximately 2−5 cm^{-1} relative to the corresponding peaks in wt (284 and 297 cm^{-1}, respectively). At higher energy, the 325−400 cm^{-1} spectral region is deconvoluted into five well-resolved peaks. The most intense band in M13V is broader and more pronounced than the corresponding peak in wt. This feature can be fit to two Gaussian bands centered at 340 and 348 cm^{-1}. Most diagnostic is a distinct three-band pattern observed in the mutant at higher energy, which is very different from wt. In the fit, three peaks located at 364, 378, and 392 cm^{-1} are identified. Particularly interesting is the intensity enhancement of the band at 392 cm^{-1} in M13V: while this feature appears as a shoulder in wt, it develops into a well-defined peak in M13V. Lastly, a weak feature at 406 cm^{-1} trailing the high-energy features is clearly resolved as a shoulder in M13V as shown in Figure 2.

The M13V/K22M double mutant has a CXXCH motif that is more rigid than that of M13V. This conclusion is again based on hydrogen exchange NMR studies.[22] Lys22 lies across the loop and is proposed to stabilize it against conformational fluctuations that lead to exchange of amide protons. However, because of its charged nature, this residue may also interact with the solvent shell of the protein. Replacing Lys22 with an amino acid containing a nonpolar side chain such as Met weakens the interaction of this residue with solvent, likely strengthening its interaction with the CXXCH loop. This interaction is proposed to stabilize the loop and augment the H-bonding interactions within the loop, yielding tighter hydrophobic packing within the CXXCH motif. The stabilized CXXCH loop in turn could induce a stronger Fe−N_{His} coordination, which is indicated by NMR results.[22] Furthermore, like in M13V, the degree of heme ruffling in the double mutant is increased.[24] The combination of an increased degree of ruffling and a stronger Fe(III)−His interaction is suggested to be the cause for a decrease in reduction potential for the double mutant (155 mV vs SHE) relative to that of wt (236 mV).[22] These structural modifications generate a NRVS spectrum of M13V/K22M that is noticeably different from that of wt as shown in Figure 2. In the 275−325 cm^{-1} spectral region, five distinct bands are resolved: the three-peak feature appearing at 290, 301, and 311 cm^{-1} now displays comparable NRVS intensities for all three bands, which is unlike that observed in wt and its M13V counterpart. In addition, a weak band becomes more prominent in the double mutant at 323 cm^{-1}. In the 325−400 cm^{-1} region, the spectral features are deconvoluted into five bands. The most prominent NRVS band occurs at 342 cm^{-1}, which is more intense than the corresponding peak in wt. A distinct shoulder appears at 354 cm^{-1}, which interestingly is not as pronounced in the NRVS spectrum of M13V as in that of wt. Further into the higher-energy region, three bands with almost equal intensity are observed at 369, 382, and 397 cm^{-1}. Importantly, *this pattern is generally very similar to that observed in the NRVS data of M13V and clearly different from that of wt.* In comparison to wt, the band at 397 cm^{-1} in M13V/K22M is more defined with a distinctively larger intensity. Finally, a weak feature is noticeable at 419 cm^{-1}, whose NRVS energy and intensity are comparable to the corresponding feature in wt.

For the A7F variant, the H-bonding interaction between the C═O group of Ala7 and the N−H group of Cys12 is proposed to be weakened or eliminated. This mutant experiences a decrease in its degree of heme ruffling of ∼0.1 Å.[21] While this change may be subtle, differences in the NRVS data between A7F and wt are apparent in Figure 2. At lower energy, the three-band spectral feature in the 250−325 cm^{-1} region is resolved into five Gaussian bands in A7F. The fifth peak within this region appears only as a shoulder in A7F, while it is a defined peak in wt (also see Figure 6). Furthermore, the peaks at 284 and 310 cm^{-1} that flank the most intense band at 297

DOI: 10.1021/bi501430z
Biochemistry 2015, 54, 1064−1076

cm^{-1} have greater intensities relative to those of the corresponding features in wt. The differences in the NRVS data are more pronounced in the higher-energy region. The 325−400 cm^{-1} data in A7F are deconvoluted into six bands. While the wt data display a shoulder at ∼330 cm^{-1}, this spectral feature is shifted to lower energy and becomes a more defined signal centered at 322 cm^{-1} in A7F. The most intense NRVS band in wt occurs at 340 cm^{-1}, which appears to be split with a weaker component at 350 cm^{-1} in A7F. The remaining spectral pattern with bands at 363, 374, 384, and 394 cm^{-1} in A7F is very similar to that of wt as shown in Figure 2. A complete list of the NRVS energies for wt and the variants is given in Table 1.

QCC-NCA Fit of the NRVS Data of *Ht* *c*-552 (see the Supporting Information for all details). The bands in the NRVS spectrum of ^{57}Fe *Ht* *c*-552 representing vibrational modes that arise from the N_{His}−Fe−S_{Met} axial unit, the heme, and the polypeptide (especially the CXXCH segment) have recently been assigned by our group.[17] The assignment has been achieved by constructing a model of the *Ht* *c*-552 active site, comprised of the heme, the axial Met, and the CXXCH loop, including the His ligand to heme. DFT was then used to calculate the force field for this model, which was subsequently refined using QCC-NCA[16] to reproduce the NRVS data of wt and isotopically labeled proteins. Table 2 shows a list of the main force constants that were adjusted during the QCC-NCA simulation. In this way, the experimental vibrational energies, NRVS intensities, and isotope shifts were well-reproduced (Figure 3). Deviations are observed in the lower-energy region (150−325 cm^{-1}), which is dominated by heme and N_{His}−Fe−S_{Met} axial ligand motions that are strongly coupled to vibrations of the polypeptide. At higher energy (325−400 cm^{-1}), the most intense NRVS features arise from in-plane (ip) iron−pyrrole stretching vibrations, ν(Fe−N_{Pyr}), and out-of-plane (oop) pyrrole tilting and swiveling modes. Beyond this region at 400−500 cm^{-1}, weaker features are attributed to pure heme modes, and mixed heme and polypeptide motions. A complete assignment of the vibrational modes in the 150−450 cm^{-1} region from our previous study on ferric *Ht* *c*-552 is available in ref 17.

Table 1. Experimental NRVS Vibrational Energies (cm^{-1}) of wt Ferric *Ht* *c*-552 and Variants M13V, M13V/K22M, and A7F from the Gaussian Deconvolution of the Experimental Data (see Figure 2)

wt	M13V	M13V/K22M	A7F
273	277	277	272
284	288	290	284
297	299	301	297
306	306	311	n/a
316	315	323	310
334	327	n/a	322
344	340	342	340
355	348	354	350
366	364	369	363
375	n/a	n/a	374
385	378	382	384
397	392	397	394
418	406	419	419
464	n/a	n/a	n/a
485	n/a	n/a	n/a

Despite the success in reproducing the experimental NRVS data of *Ht* *c*-552 with our QCC-NCA simulation in previous work, discrepancies between the fit and the experimental data remained (see Figure 3). For example, the vibrational energies of the "three-band" feature in the 250−325 cm^{-1} region are shifted to lower energy by ∼15 cm^{-1} compared to experiment. In addition, a weak feature at 316 cm^{-1} in this region is noticeable in the simulated spectrum but is absent in the experimental NRVS data. Finally, the DFT-optimized structure of the CXXCH loop in the model used in ref 17 shows deviations from the *Ht* *c*-552 crystal structure (see below). These inconsistencies prompted us to investigate whether a more accurate model of the active site would reproduce the wt NRVS data with even better accuracy, which is important for the exploration of how the NRVS data of mutants M13V, M13V/K22M, and A7F investigated here can be reconstructed from the wt spectrum. Thus, a model of the *Ht* *c*-552 active site with a conformation of the CXXCH loop that better mimics the protein crystal structure was generated (see Figure 1). Details are given in the Supporting Information. The new fit leads to noticeable improvements in the 250−325 cm^{-1} region as shown in Figure 3. On the basis of the agreement between the experiment and the current QCC-NCA simulation, the NRVS spectrum of ferric *Ht* *c*-552 can be assigned (see Tables S4 and S5 of the Supporting Information). Notably, compared to the previous model,[17] the vibrational assignments in the 340−425 cm^{-1} region are identical, but some changes are noted for the vibrational features in the 250−325 cm^{-1} region (see the Supporting Information for details).

Effect of Individual Structural Changes in *Ht* *c*-552 on the NRVS Data. To first understand how the key structural modifications of the *Ht* *c*-552 active site observed in the mutants affect the NRVS spectra, the obtained (QCC-NCA optimized) force field of the wt active site model was used, and the effect of the variation of the following (structural) parameters on the simulated spectra was tested: (a) the H-bonding strength within the pentapeptide loop, (b) the flexibility/stiffness of the CXXCH linker, (c) the Fe−N_{His} bond strength, and (d) the degree of distortion of the heme from planarity. The choice of these parameters stems from the proposed structural alterations in variants M13V, M13V/K22M, and A7F relative to wt as described above.[21,22,24] To test effects (a)−(c), the force constants corresponding to these modifications were adjusted in the *Ht* *c*-552 force field, and the NRVS spectrum was then recalculated (Table 2). For effect (d), the force constants were frozen but the structure of the heme macrocycle was distorted along the ruffling coordinate (see Figure S1 of the Supporting Information), and then the NRVS spectrum was recalculated. The vibrational energies quoted in this section therefore refer to those obtained from the QCC-NCA simulations [comparing simulated wt energies to those obtained for (a)−(d)] and **not** the experimental data.

(a). H-Bonds within the CXXCH Pentapeptide Loop. As mentioned above, the two H-bonds that form between the C═O group of Cys12 and the N−H groups of Cys15 and His16 are potentially important in maintaining the conformation of the CXXCH loop (see Figures 1 and 4). For mutants M13V and M13V/K22M, these H-bonding interactions have been proposed to increase as part of an overall tightening of the CXXCH loop.[22] To simulate this effect, the force constants corresponding to these two H-bonding interactions were increased by ∼25% (to model the single mutant) and ∼55% (for the double mutant) relative to wt. However, as is evident

DOI: 10.1021/bi501430z
Biochemistry 2015, 54, 1064−1076

Table 2. Selected Force Constants[a] of Ferric *Ht* c-552 Invoked in the Fit of the wt Protein NRVS Data, Based on the BP86/LanL2DZ* Result (using the QCC-NCA approach)

force constant[a]	BP86/LanL2DZ*	QCC-NCA
Fe−S_{Met} [1]	0.7905	0.8404
Fe−N_{His} [17]	1.4835	1.2493
Fe−N_{Pyr} [13−16]	1.6094, 1.6255, 1.6396, 1.6919	1.6981, 1.6771, 1.6961, 1.8058
ν(His)	4.4768, 3.6772, 5.5075, 6.3193	4.8030, 3.7548, 5.4300, 6.8063
δ(pp)	0.7940, 0.8429, 0.7663, 0.4935, 0.7320, 0.6208, 0.5948, 0.6621, 0.5463, 0.8197, 0.6601, 0.5861, 0.5529, 0.7100, 0.7293, 0.6534	0.9057, 0.9968, 0.9963, 0.6531, 0.8320, 0.8208, 0.2548, 0.8921, 0.6463, 0.8197, 0.5601, 0.6001, 0.5529, 0.7100, 0.7893, 0.4034
δ(His) [371, 372, 377, 378, 385, 391, 397]	0.9225, 0.7040, 0.4785, 0.5857, 0.5743, 0.9837, 0.7051	0.8901, 0.8640, 0.4356, 0.5001, 0.7027, 1.0885, 0.8095
δ(Met) [163, 181]	0.6771, 1.1543	0.8871, 0.9553
τ(Met) [459−461]	0.0797, 0.0794, 0.1711	0.0681, 0.1190, 0.0720
τ(Fe−S_{Met}), τ(Fe−N_{His}) [458, 462]	0.1742, 0.7799	0.3879, 0.8214
τ(His)	0.1931, 0.9253, 1.4613, 1.1402, 0.2102, 3.2671, 1.3095, 0.1846	0.1358, 0.8600, 1.0601, 0.6909, 0.2142, 3.2152, 1.1596, 0.1846
τ(pp)	0.6082, 0.2192, 0.2689, 0.7477, 0.3144, 0.3300, 0.4773, 0.2566, 0.2562, 0.2954, 0.2508	0.5540, 0.3329, 0.2918, 0.2999, 0.1451, 0.1957, 0.3853, 0.1913, 0.2549, 0.3168, 0.2727

[a]The units of the force constants are mdyn/Å for stretching and mdyn·Å for bending and torsional internal coordinates. For a complete list of force constants, see the Supporting Information.

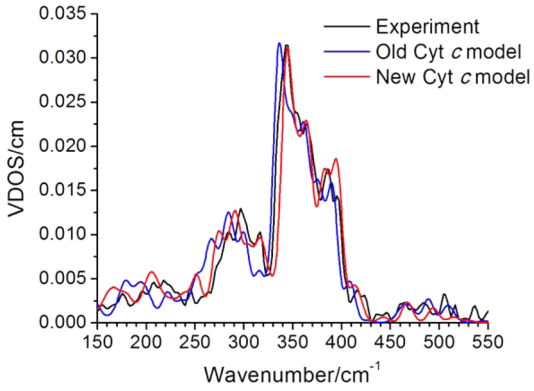

Figure 3. Experimental and QCC-NCA simulated NRVS data of ferric wt *Ht* c-552 using the previous model[17] and the new and improved model (this work).

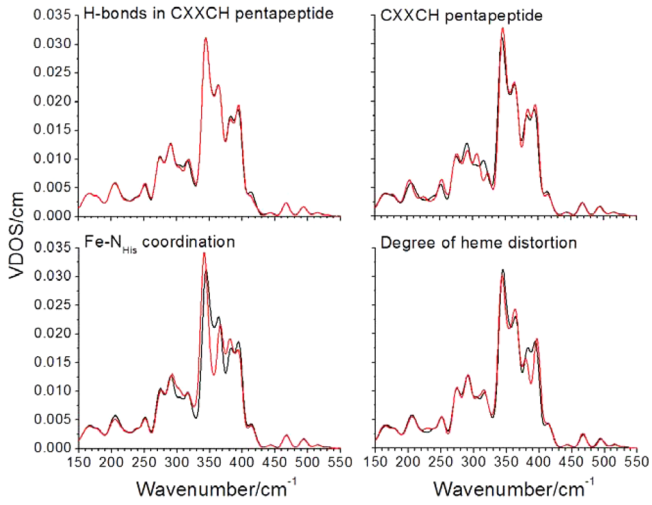

Figure 5. Simulated NRVS spectra of ferric *Ht* c-552 as a function of modifying the H-bonding interaction in the CXXCH loop, the CXXCH pentapeptide stiffness, the Fe−N_{His} interaction (stretching and torsion), and the degree of heme ruffling. The black and red spectra correspond to the QCC-NCA simulations before and after incorporating the structural modifications, respectively.

from Figure 5, this causes very minor modifications of the simulated NRVS data: the peak at 316 cm^{-1} shifts very slightly to higher energy, and the intensities of the bands at 380, 396, and 412 cm^{-1} show very small alterations. Hence, the two H-bonds within the CXXCH loop play only a minor role in the observed variations of the NRVS data in the mutants. This

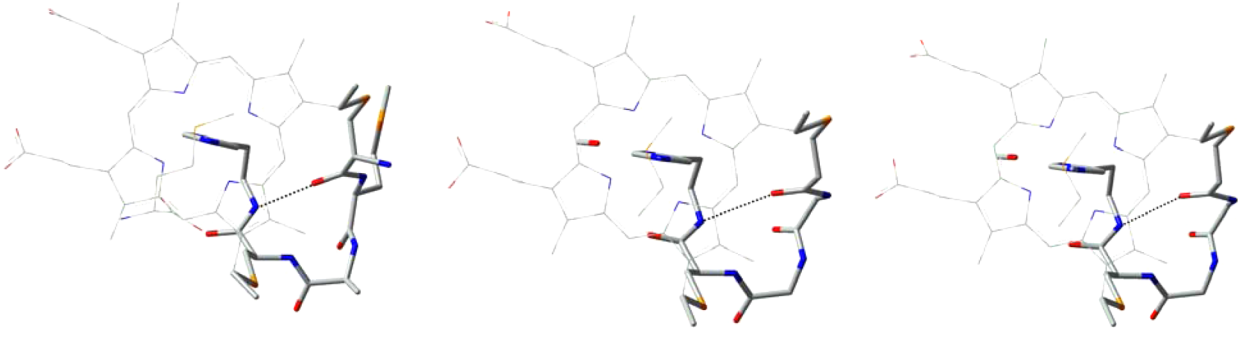

Figure 4. Structure of the active site model of ferric *Ht* c-552 (left, PDB entry 1YNR), optimized geometry of the original model (middle), and optimized structure of the new model (right). The atoms of the axial Met are shown in the background as stick models. The pictorial representations focus on the Cys12-Met13-Ala14-Cys15-His16 pentapeptide on the proximal side of the heme. The yellow, red, blue, and gray tubes represent sulfur, oxygen, nitrogen, and carbon, respectively.

DOI: 10.1021/bi501430z
Biochemistry 2015, 54, 1064−1076

further indicates that these interactions are weak and likely not important for maintaining the conformation of the pentapeptide loop in the proteins.

(b). Flexibility of the CXXCH Pentapeptide Loop. Unlike the H-bonds, adjustment of the force constants of the CXXCH pentapeptide loop to increase its rigidity leads to distinct modifications of the NRVS data as shown in Figure 5. Compared to the single mutant, the CXXCH loop of the double mutant is expected to be even stiffer with Met at position 22. While the force constants corresponding to the stretching modes in the loop have a very minimal effect, the bending and torsional modes alter the NRVS spectra in a distinct way. On average, the bending and torsional force constants of the loop region in M13V were set to be slightly lower than those in M13V/K22M to take into consideration the previous conclusion that the CXXCH loop is more rigid in the double mutant (see Table S6 of the Supporting Information).[22] The force constants from two specific residues are particularly important for fine-tuning the mutant spectra: Cys12 and His16. For example, the $\delta(C_a-S_1-C)_{PyrI}$ bending mode of Cys12 modulates the intensity of the main band at 344 cm^{-1}. In fact, in NRVS data of both mutants, the peak at 344 cm^{-1} is more intense than the corresponding band in wt. For M13V/K22M, Met22 lies across the CXXCH loop, possibly further influencing Cys12 compared to the single mutant, resulting in the observed spectral changes.[a]

The other set of force constants that modifies the NRVS spectra of both variants arises from His16. Adjusting the force constants of the torsional and bending modes of this residue accurately replicates the 275–325 cm^{-1} NRVS region in the mutant spectra (see Figure 5). Importantly, tweaking the His16 force field generates the weak feature at 323 cm^{-1} that is distinct in the double mutant. It is notable that the intensities of the bands at higher energy (e.g., 365, 380, 396, and 412 cm^{-1}) are also affected by changes within the loop, highlighting the strong mixing between heme and polypeptide vibrations. The key role of His16 can be traced back to a previous study of hydrogen exchange rates or "protection factors", which reveal the free energy of the CXXCH conformational fluctuations that lead to exchange of amide protons.[22] For M13V/K22M, the level of protection of His16 dramatically increases by 3 orders of magnitude relative to wt. This emphasizes the effect of residues 13 and 22 on the local loop conformational fluctuations and the loop stiffness, especially affecting Cys12 and His16. The NRVS results provide further support for these ideas.

(c). Fe–N_{His} Bond Strength. The Fe–N_{His} coordination in Cyt *c* is directly influenced by the H-bonding interaction and CXXCH pentapeptide flexibility. Compared to wt, the single and double mutants have a tighter hydrophobic packing around the heme as discussed above. The decrease in the loop conformational fluctuations of the variants is proposed to yield a stronger Fe–N_{His} coordination.[22] To simulate this effect, the force constants corresponding to the Fe–N_{His} stretch and torsion were modified in the force field of the variants. To obtain a reasonable match with the NRVS data while adhering to the proposed changes in Fe–N_{His} coordination, the Fe–N_{His} stretching force constant was increased by approximately 5 and 6% for the single and double mutant, respectively. In addition, the force constants of the τ(Fe–N_{His}) torsional internal coordinate were reduced. The features in the NRVS data that are particularly sensitive to the Fe–N_{His} stretching force constant are the bands at 276 and 304 cm^{-1}, and relatively smaller changes are observed for the features at 365 and 383 cm^{-1}. On the other hand, the Fe–N_{His} torsional force constant greatly affects the features at 344 and 365 cm^{-1} and, to some extent, the bands at 380 and 394 cm^{-1}. The cumulative effects of the Fe–N_{His} coordination (stretching and torsion) are presented in Figure 5. The variants show a very characteristic three-band pattern in the 360–400 cm^{-1} region (see Figure 2), which can be reproduced only by adjusting the Fe–N_{His} properties. While the ν(Fe–N_{His}) stretching mode is predominantly distributed over the 145–325 cm^{-1} region, the τ(Fe–N_{His}) torsional vibrations are spread throughout the 340–400 cm^{-1} spectral region (Table S5 of the Supporting Information).

(d). Heme Ruffling. On the basis of prior observations of reduction potential changes that were related back to the degree of heme distortion,[22] it is interesting to investigate how heme conformation affects the NRVS data. NMR and EPR spectra suggest that the degree of heme ruffling in M13V and M13V/K22M increases, and this was further tested in our QCC-NCA simulations. In both mutants, the increased rigidity of the CXXCH loop has been proposed to enhance the loop's buckling force, which potentially amplifies the amount of heme distortion and, in this way, could decrease the heme reduction potential.[22] For the QCC-NCA simulations, the conformation of the heme was changed, but force constants were not altered between variants. The structure of the *Ht c*-552 model used in simulating the enhanced effect of heme distortion is presented in Figure S1 of the Supporting Information. As shown in Figure 5, the feature that is mainly affected by the heme conformation is the band at 396 cm^{-1}, which becomes more prominent with an increase in the degree of ruffling. Heme distortion therefore plays an important role in determining the features in the high-energy region (350–400 cm^{-1}) of the NRVS spectra (see below).

(e). Summary. The QCC-NCA simulations on each structural change proposed for the *Ht c*-552 mutants studied in this work support the following key observations.

(i) Varying the strength of the H-bonds across the pentapeptide loop in itself has no measurable effect on the NRVS data.

(ii) For M13V and M13V/K22M, the observed changes in the 275–325 cm^{-1} spectral region can be traced back to increases in loop stiffness, particularly affecting Cys12 and His16.

(iii) The characteristic three-band pattern in the 360–400 cm^{-1} region of the M13V and M13V/K22M NRVS data can be reproduced by adjusting the Fe–N_{His} bonding properties.

(iv) An increased degree of heme ruffling further affects the high-energy region of the NRVS data of the mutants, particularly in the 380–400 cm^{-1} range.

Therefore, NRVS is able to specifically probe changes in loop stiffness, Fe–N_{His} interaction, and heme conformation in Cyt c, as evidenced by specific spectral changes that are detected in response to alterations of these properties. This information is very difficult to obtain experimentally and otherwise requires the application of a number of different spectroscopic methods.[21,24,34,39,40] These results illustrate the potential of NRVS to reveal subtle and specific features of active site structure and dynamics in iron-containing proteins more generally.

Interpreting the NRVS Spectra of M13V, M13V/K22M, and A7F. On the basis of the results described above,

DOI: 10.1021/bi501430z
Biochemistry 2015, 54, 1064–1076

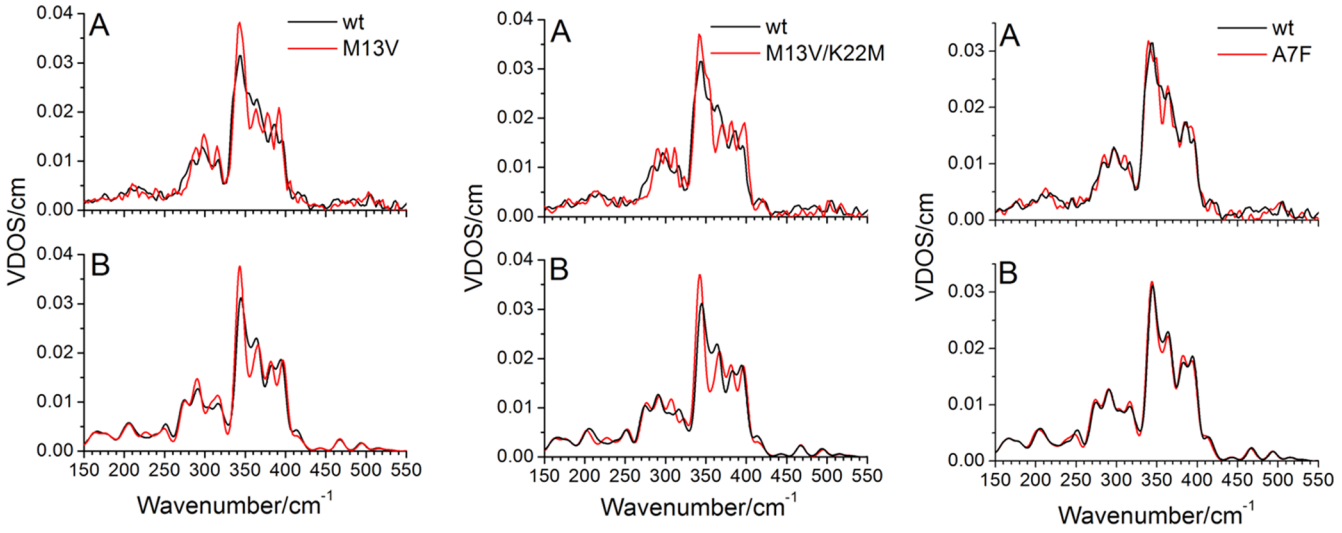

Figure 6. Experimental (A, top row) and QCC-NCA simulated (B, bottom row) NRVS data of ferric wt *Ht c*-552 (black spectra) and variants (red spectra) M13V (left column), M13V/K22M (middle column), and A7F (right column) as indicated.

systematic simulations of the NRVS data of M13V and M13V/K22M can be performed, and the results can further be correlated to the data obtained for A7F. In general, several key features are conceived from this work: (1) the strength of the Fe−N_{His} bond is directly related to the extent of ruffling; (2) the Cys12-to-heme linkage strongly influences the intensity of the band at ∼340 cm^{-1} and is directly related to the CXXCH loop stiffness; (3) the degree of heme distortion is elucidated through the prominence of the band at ∼390 cm^{-1}. Details of the contributions of a particular vibrational mode to a spectral NRVS feature, and its correlation with the protein structure, are presented below.

M13V NRVS Data. Figure 6 shows very good agreement between the experimental NRVS data (top panel) and the QCC-NCA fit (bottom panel) of M13V. In the 250−325 cm^{-1} region, the intensity of the NRVS features is generally higher in the M13V mutant than in wt. QCC-NCA reveals increased contributions from vibrational motions arising from the N_{His}−Fe−S_{Met} axial unit and ν(Fe−N_{Pyr}) (Pyr = pyrrole) in M13V compared to wt, leading to larger Fe displacements as reflected by an enhancement of the peak intensities of M13V in this region. In the 325−400 cm^{-1} range, the most intense feature is fit to two Gaussian bands centered at 340 and 348 cm^{-1}, which formally contain 18 and 16% ν(Fe−N_{Pyr}) character, respectively. These two features correspond to the bands at 344 and 355 cm^{-1} in wt, respectively, both of which have slightly less ν(Fe−N_{Pyr}) contribution combined. The cumulative contributions from the ip [e.g., ν(Fe−N_{Pyr})] and oop (e.g., Pyr tilt) heme motions to the Fe displacement in M13V account for the difference in intensity of the main band relative to wt. A key internal coordinate that modulates the intensity of this band is the $\delta(C_a{-}S_1{-}C)_{PyrI}$ bending mode of Cys12, which induces variations with respect to the amount of mixing of this feature with CXXCH loop vibrations. In the higher-energy region, a well-defined three-band pattern is observed with peaks at 364, 378, and 392 cm^{-1} that is unique to the M13V and M13V/K22M (see next paragraph) mutants, and not observed in wt. QCC-NCA indicates that these bands have significant contributions from pyrrole oop motions and the ν(Fe−N_{Pyr}) stretch. The disparity in the band intensities between M13V and wt within this region may be attributed to a greater contribution of pyrrole tilting/swiveling modes in M13V. Furthermore, to properly simulate this region in the mutant spectra, the Fe−N_{His} bond (force constant) had to be strengthened, the τ(Fe−N_{His}) force constant was reduced, and the degree of heme ruffling had to be enhanced. This is fully consistent with the proposed structural changes created by mutating Met13 to Val (see above). QCC-NCA simulations demonstrate that the feature at 392 cm^{-1} becomes more prominent when the degree of heme ruffling is augmented (−1.0 Å) relative to the degree of heme distortion in wt (−0.78 Å). Prior NMR and EPR studies had demonstrated that the heme is more ruffled in M13V.[22,24] Our NRVS results provide support for this idea. The complete list of force constants used to simulate the spectrum of M13V is presented in Table S6 of the Supporting Information.

M13V/K22M NRVS Data. The experimental and simulated NRVS data of M13V/K22M are again in very good agreement with experiment as shown in Figure 6. In the 250−325 cm^{-1} energy region, the peaks at 290, 301, and 311 cm^{-1} are more similar in intensity to each other compared to wt, which is reproduced by the QCC-NCA fit. This change in intensities is accompanied by a shift of the band at 316 cm^{-1} in wt to higher energy in the mutant (323 cm^{-1}). QCC-NCA reveals that this band has considerable axial ligand character [34% τ(His) and 13% δ(His) modes], but nevertheless, these contributions are decreased compared to those in wt. This feature is very sensitive to modifications involving the τ(His) and δ(His) force constants. In M13V/K22M, the intensity reduction of this band is due to the redistribution of the τ(His) and δ(His) internal coordinates over adjacent lower-energy modes. At higher energy, the most intense NRVS spectral feature at 342 cm^{-1} is substantially more intense than the corresponding band in wt, because of an increase in ν(Fe−N_{Pyr}) character (26%) and additional contributions from oop motions (similar to the case for M13V). Like in M13V, the $\delta(C_a{-}S_1{-}C)_{PyrI}$ internal coordinate modulates the intensity of the 342 cm^{-1} feature, and the corresponding force constant for this internal coordinate from the QCC-NCA fit of M13V/K22M is comparable to that of the M13V fit (see Table S6 of the Supporting Information), in accordance with the comparable intensity of this feature in spectra of both mutants. Further into

DOI: 10.1021/bi501430z
Biochemistry 2015, 54, 1064−1076

the 350−400 cm^{-1} region, a characteristic three-band spectral pattern emerges with bands at 369, 382, and 397 cm^{-1}, which is very similar to that observed for M13V (see Figure 6). By strengthening the Fe−N_{His} bond, reducing the τ(Fe−N_{His}) force constant, and enhancing the degree of heme distortion, we properly simulated the high-energy spectral features in M13V/K22M. As observed for M13V, the peak at 397 cm^{-1} becomes prominent when the heme is more ruffled. This supports the idea that the heme in M13V/K22M is more distorted than in wt.[22] Figure S1 of the Supporting Information shows a structure of the model used to replicate the degree of heme ruffling in both M13V and M13V/K22M. In the QCC-NCA simulations, the degree of heme distortion in both single and double mutants is similar. However, compared to M13V, simulation of the NRVS data of the double mutant required a more rigid loop, and a slightly stronger Fe−N_{His} bond and H-bonding network within the CXXCH loop. Table S6 of the Supporting Information shows the complete list of the force constants used to simulate the spectrum of M13V/K22M.

A7F NRVS Data. The structural modifications caused by mutating Ala7 to Phe are the opposite of those created in M13V and M13V/K22M; notably, the A7F mutation decreases the degree of heme ruffling, whereas the M13V and M13V/K22M mutations increase the degree of ruffling. Most significantly, to reproduce the experimental NRVS data of A7F, the amount of heme distortion has to be reduced, the Fe−N_{His} bond has to be weakened, and, in addition, the CXXCH loop is made more flexible by decreasing the polypeptide bending force constants (Table S6 of the Supporting Information). Among these structural changes, the degree of heme ruffling was the most significant factor in simulating the overall NRVS features in A7F; however, slightly changing the Fe−N_{His} bond and polypeptide bending contributions was necessary to fine-tune the spectrum. A structure of the model used to mimic the degree of heme ruffling in A7F is presented in Figure S1 of the Supporting Information. The resulting NRVS simulation is in good agreement with the experimental data as shown in Figure 6. In the lower-energy region of the experimental NRVS data for A7F, the bands at 284 and 310 cm^{-1} show intensities slightly larger than those of wt. QCC-NCA establishes that these features have slightly greater contributions from axial N_{His}−Fe−S_{Met} vibrations and polypeptide motions compared to their wt counterparts, which causes these spectral changes. In the 325−400 cm^{-1} region, the band at 350 cm^{-1} is quite intense in A7F. This mode has a contribution from δ(Met) slightly greater than that in wt, which may account for the increased intensity in the mutant spectrum. Toward higher energy, the band at 365 cm^{-1} is clearly more prominent in A7F but not necessarily more intense than the corresponding peak in wt. To fit this peak in the mutant spectrum, the force constants of the τ(Fe−N_{His}) and ν(Fe−N_{His}) internal coordinates had to be slightly reduced. These results support the idea that mutating Ala7 to Phe results in a weaker Fe−N_{His} interaction. Finally, while the band at 394 cm^{-1} is a pronounced peak in M13V and M13V/K22M, and a weak band in wt, this feature almost coalesces with the adjacent band at 384 cm^{-1} in A7F. As discussed above, this band is sensitive to the degree of heme distortion. In the QCC-NCA simulation of A7F, the amount of heme ruffling was reduced from −0.78 to −0.65 Å (relative to the Cyt *c* model which represents wt) to approximately mimic this band (Table S2 of the Supporting Information), although the fit in this energy region is not fully accurate. We believe that this might be due to other forms of slight heme distortions, which were not matched in the fit. In addition, it is proposed that mutating Ala to Phe at position 7 weakens or removes the H-bond formed between residue 7 and the amide N−H group from Cys12.[21] Because our model does not contain residue 7, we cannot directly verify the effect of this interaction on the simulation. Nevertheless, our studies clearly support an overall reduction in the degree of heme ruffling in A7F (compared to wt) when the H-bonding interaction between the C═O group of Ala and the N−H group of Cys12 is eliminated. Table S6 of the Supporting Information lists the complete set of force constants utilized to replicate the NRVS data of A7F.

One of the most important outcomes of this analysis is the finding that a decrease in the rigidity of the CXXCH loop results in (1) a weaker Fe−N_{His} interaction, presumably because of the pentapeptide's tendency to "shift" away more readily from the heme iron center, and (2) a decreased amount of heme ruffling due to a reduced pentapeptide buckling force that supposedly influences heme distortion. These overall structural changes are apparent in the series of Cyt *c* variants investigated in this work, and they distinctively influence the vibrational properties and dynamics of the heme.

DISCUSSION

Our results establish that NRVS data for wt ferric *Ht* Cyt *c* and variants M13V, M13V/K22M, and A7F can directly elucidate subtle structural alterations in the protein active site associated with these specific point mutations. This is demonstrated by distinct peak shifts and intensity changes in the NRVS data throughout the 250−450 cm^{-1} region, even in the case of variants with seemingly conservative mutations (e.g., Met13 to Val) (Figure 6). Our results provide a direct link between the structural changes in the mutants and specific spectral changes observed in the NRVS data. Hence, NRVS could be used to identify such structural changes in other active site mutants and relate them back to changes in the properties of the heme. Because the subtle structural effects induced by mutation influence vibrational dynamics in *Ht c*-552 as shown here, they may also have an effect on protein function. As demonstrated in this work, vibrational dynamics of the heme are best revealed by NRVS rather than more conventional techniques such as resonance Raman spectroscopy (see Results). In this section, we discuss structural and functional [e.g., reduction potential, biogenesis, and electron transfer (ET)] implications of our results, presented in this paper.

CXXCH Pentapeptide Modification Response in Variants. The 275−325 cm^{-1} NRVS region is primarily sensitive to variations in the CXXCH loop conformation, although the 325−450 cm^{-1} region, which is dominated by in-plane (ip) and out-of-plane (oop) heme vibrations, also displays spectral shifts in response to pentapeptide loop modifications (Figures 5 and 6). This emphasizes that vibrational dynamic couplings between the heme and the CXXCH loop are substantial in Cyts *c*, as recently reported by us.[17]

Structural Implications. Our simulations indicate that the effect of the H-bonds across the pentapeptide loop on the NRVS data is very subtle (Figure 5), suggesting that these interactions might not play a key role in the loop structure. Instead, these interactions make a small contribution to the overall rigidity of the pentapeptide arm. This is in contrast to previous work on Ni Cyt *c* where it was concluded that the H-bonds play an important role in compressing the pentapeptide

DOI: 10.1021/bi501430z
Biochemistry 2015, 54, 1064−1076

loop segment.[41] Unlike the effect of the H-bonds across the loop, significant spectral shifts arise from modulating the flexibility of the CXXCH arm, in particular the $\delta(C_a-S_1-C)_{PyrI}$ internal coordinate from Cys12, and the torsional and bending modes of His16 (Figure 5). While the pentapeptide predominantly affects the 250−325 cm^{-1} region, the main NRVS feature at 344 cm^{-1} and the shoulder at 355 cm^{-1} are particularly sensitive to the $\delta(C_a-S_1-C)_{PyrI}$ Cys12 bend (Figure S4 of the Supporting Information). The 344 and 355 cm^{-1} features are assigned to the two main components of the E_u-symmetric (in ideal D_{4h} symmetry) ip $\nu(Fe-N_{Pyr})$ stretching mode. The spectral intensity redistribution in this region varies among mutants, reflecting variations in the loop structure that affect the $\delta(C_a-S_1-C)_{PyrI}$ Cys12 bending mode. The proximal His16 is strategically positioned within the active site such that it provides three essential structural features: (1) it forms the terminal residue in the pentapeptide segment; (2) it donates a H-bond to the backbone carbonyl of Pro25; (3) it coordinates to the Fe center as one of the axial ligands. Variation of the His16 force field yields the unique, weak feature at 323 cm^{-1} distinct to the M13V/K22M NRVS data and is required to create the characteristic "three-band pattern" of the M13V mutants in the 360−400 cm^{-1} range. This underlines the importance of this residue for the structural features of the loop and the vibrational dynamics of the heme. A previous study of the M13V and M13V/K22M mutants found suppressed hydrogen exchange between the CXXCH amide protons and solvent, which was thought to be caused by an increase in the level of protection of His16 brought about by the increased rigidity of the loop in the variants.[22] These ideas are clearly supported by the NRVS data presented here. In M13V/K22M, Val13 packs well into the pentapeptide, stabilizing the key interactions of Cys15 and His16 with Cys12. In addition, Met22 lies across the CXXCH loop, acting like an anchor that keeps the pentapeptide from undergoing conformational fluctuations that lead to the exchange of amide protons. This double mutation therefore augments the stiffness of the linker arm, which is otherwise only partially rigid in M13V (relative to M13V/K22M), as shown by enhanced levels of protection for the double mutant.[22]

Aside from being the terminal residue in the pentapeptide segment that plays a fundamental role in fine-tuning the low-energy vibrations of the *Ht c*-552 heme, His also donates a H-bond to the C═O group of Pro25, with an oxygen−nitrogen distance of ∼2.8 Å.[42] In heme proteins, this noncovalent interaction affects the electron donating properties of His, which also controls redox potential, as discussed below.[43−45] Modifying the force constant associated with this H-bonding interaction induces a small intensity change in the 160−220 cm^{-1} spectral region (Figure S5 of the Supporting Information), which is caused by subtle changes in the vibrations of the axial (His)N−Fe−S(Met) unit. Hence, NRVS does not seem to be particularly sensitive to small changes in the H-bond, implying that this hydrogen bond has an only small effect on the heme properties in Cyt *c*.

Functional Implications. The heme reduction potential, which correlates with hydrogen exchange rates of the CXXCH amide protons as described above, shows the following systematic trend: wt (236 mV) > M13V (177 mV) > M13V/K22M (155 mV).[22] The significant decrease in reduction potential exhibited by the double mutant is a result of fundamental alterations in the heme pocket structure, and not electrostatic perturbations caused by the mutation.[22] Beyond the CXXCH rigidity, other alterations of the active site, likely linked to the increased rigidity of the loop, contribute to the change in reduction potential. This includes the $Fe-N_{His}$ coordination and heme distortion, which are discussed below.

While Cyts *c* have long been known to function as electron transfer proteins, the detailed mechanism of ET is still actively being investigated. One factor that is crucial for ET in proteins is vibrational excitation (thermal energy that is converted into vibrational excitation via inelastic collision processes), which is described by Marcus theory[46] as the energy required for the system to reach the transition state for ET. During formation of the protein−protein complex, which occurs in the area of pyrrole II of the heme, very close to the CXXCH loop,[47] the heme−pentapeptide vibrational couplings may affect Cyt *c* ET function in different ways. In particular, conformational changes of the CXXCH pentapeptide may lead to the modulation of the vibrational Eigenstates and the structure of the heme. Here, the vibrations associated with the CXXCH segment, modulated by conformational changes of the loop, may influence the ET process by localizing the heme at an energy minimum that is optimal for ET when in complex with an ET partner, thus influencing the reorganization energy of the ET process and the barrier for electron transfer. On the basis of our NRVS simulations, such modulations could arise from the bending and torsional modes of the pentapeptide in the 250−325 cm^{-1} region (Tables S4 and S5 of the Supporting Information). Via the adjustment of the CXXCH loop flexibility through Cys12 and His16, and the $Fe-N_{His}$ interaction, the loop can modulate the vibrational dynamics of the heme to optimally condition it for ET. In a similar way, modulation of the heme vibrations, coupled to vibrational excitation, could be used by the protein to dynamically localize the hole/electron to be transferred in ET on pyrrole II of the heme, directing the hole/electron toward the Cyt *c* redox partner.

The CXXCH pentapeptide also has a central role in Cyt *c* biogenesis, where this conserved motif is used for protein−protein recognition. For example, in eukaryotes (e.g., *Equus caballus*), holocytochrome *c* synthase (HCCS) catalyzes the attachment of heme to apoCyt *c* during the process of Cyt *c* maturation. Importantly, it has been shown that His in CXXCH helps orchestrate heme recognition, attachment, and release from HCCS upon formation of the protein−protein complex.[48] His achieves this by providing the second axial ligand to the heme at the HCCS active site, positioning the thiols in the pentapeptide loop to be in the proximity of the two heme vinyl groups, and pulling the heme away from the HCCS active site, therefore releasing (and forming) holoCyt *c*.[49] Indeed, mutation of the Cyt *c* axial His residue to Met, Lys, or Arg generates variants that fail to attach heme, further establishing the necessity of His in Cyt *c* biogenesis.

Effect of $Fe-N_{His}$ Coordination. The rigidity of the CXXCH segment likely affects the $Fe-N_{His}$ interaction, and the NRVS data in the 145−325 and 340−400 cm^{-1} regions are in fact very sensitive to changes in $\nu(Fe-N_{His})$ stretching and $\tau(Fe-N_{His})$ torsional force constants.

Structural Implications. The characteristic "three-band pattern" in the 360−400 cm^{-1} region of the M13V mutant spectra in particular can only be generated by changing the loop stiffness and Fe−His coordination. Our simulations reveal that M13V/K22M has an $Fe-N_{His}$ bond strength slightly greater than that of M13V. This is consistent with the idea that tighter hydrophobic packing (greater rigidity) within the linker arm results in a stronger $Fe-N_{His}$ coordination.

DOI: 10.1021/bi501430z
Biochemistry 2015, 54, 1064−1076

Functional Implications. The lower reduction potential of the double (as well as the single) mutant over wt[22] can be explained in terms of the Fe−N_{His} bond strength, where an increase in the level of His → Fe donation stabilizes the ferric state and lowers the reduction potential. The structural correlation between CXXCH rigidity and Fe−N_{His} interaction is consistent with observations in mitochondrial ferric Cyt b_5, which has a tightly packed heme active site that is suggested to produce a stronger Fe−N_{His} coordination compared to that of microsomal ferric Cyt b_5.[50] Our QCC-NCA simulations for the A7F variant are consistent with this trend. In this case, the ν(Fe−N_{His}) and τ(Fe−N_{His}) force constants had to be reduced, demonstrating that the Fe−N_{His} coordination in A7F is somewhat weaker than in wt or the M13V variants. From our results, the reduction potential of A7F can be expected to be slightly higher than that of wt as a result of slightly weaker His coordination. Importantly, NMR analysis of *Ht c*-552 A7F also indicates that heme distortion decreases by ∼0.1 Å in this variant, which can further affect redox potential.[21] Taken together, *these experimental results and our QCC-NCA simulations implicate a direct correlation between CXXCH rigidity, Fe−N_{His} interaction and heme distortion, and reduction potential.*

Role of Heme Conformation. Our QCC-NCA simulations reveal that the 380−400 cm^{-1} region, in particular the band at ∼395 cm^{-1}, is diagnostic of the degree of heme distortion (Figure 5). The more distorted the heme, the more prominent this high-energy band becomes (and vice versa).

Structural Implications. In Cyt *c*, the dominant oop heme distortion is ruffling,[51] in which the Fe−N(pyrrole) bonds are twisted in alternate directions (Figure S1 of the Supporting Information). The prominent band at ∼395 cm^{-1} observed in the spectra of M13V and M13V/K22M clearly indicates a heme more ruffled than that of wt. The amplified heme distortion in these variants can be related to their rigid CXXCH linker arms and strong Fe−N_{His} coordination. Previous studies of microperoxidases show that the CXXCH pentapeptide is adequate to generate increased distortion of the heme toward the ruffled conformation.[52,53] As opposed to the single and double mutants, QCC-NCA analysis indicates that the heme in A7F (−0.65 Å) is less ruffled than that of wt (−0.78 Å). Our results are consistent with previous NMR and EPR analyses supporting a more planar heme structure in A7F.[21] This conclusion is additionally supported by structural studies of the structurally homologous wt *Pseudomonas aeruginosa* cytochrome *c*-551 (*Pa c*-551) and the corresponding F7A mutant.[54]

Functional Implications. The amplified heme distortion makes additional contributions to changes in redox potential (besides the change in Fe−N_{His} interaction). The extent of heme distortion correlates with reduction potential as follows: M13V/K22M (155 mV, most ruffled) < M13V (177 mV) < wt (236 mV, least ruffled).[22] This indicates a role of ruffling in ET processes. A recent study of wt *Pa c*-551 (less ruffled) and its F7A mutant (more ruffled) using vibrational coherence spectroscopy demonstrates that the extent of heme ruffling can be monitored via the ruffling-sensitive mode γ_a that occurs in the lower-frequency region (58 and 52 cm^{-1} for wt and F7A, respectively).[55] Interestingly, the photoreduction cross section in wt *Pa c*-551 is nearly 2 orders of magnitude greater than that of F7A. The factors that potentially reduce the electron transfer rate (which directly correlates with the photoreduction cross section) in F7A relative to wt are electronic coupling, reorganization energy (which correlates with the Marcus barrier), and inelastic processes that lead to excitation of the ruffling vibration that effectively increases the Marcus barrier.[55] In the work presented here, we note that higher-energy vibrations of the heme (∼390 cm^{-1}) are also sensitive to heme ruffling. From a structure−function standpoint, the degree of heme distortion plays an important role in optimizing the energy of the vibrational modes that encompass the low- and high-frequency regions. When Cyt *c* is bound to the mitochondrial membrane, the heme flattens to a more planar conformation as demonstrated by a weakening of a mode related to the ruffling distortion,[56] thus increasing the level of electronic coupling to allow Cyt *c* to transfer electrons more readily than when it is free in the cytoplasm. Putting these ideas into the context of the results reported here, we have demonstrated how very subtle changes around the CXXCH loop region can influence heme ruffling and vibrational dynamics. Because the CXXCH segment forms a portion of the known protein−protein interaction interface in Cyt *c*, it thus can be expected that binding to a partner protein will result in changes in the CXXCH residues that will be transmitted to the heme via the vibrational coupling between the CXXCH segment and the heme. From a structural standpoint, binding of a protein to Cyt *c* could potentially affect heme ruffling by modulating the structure of the loop. If the resulting change causes the heme to flatten as is seen upon binding to mitochondrial membranes, binding could potentially lead to an increase in ET rate.

Beyond modulating the redox potential and ET rates, the heme conformation plays a role in folding of the enzyme to its native structure during biogenesis. During this process, HCCS catalyzes the binding of heme to apoCyt *c*, subsequently releasing holoCyt *c*. It was recently demonstrated that heme distortion (puckering) controls the dissociation of holoCyt *c* from the complex, thus facilitating the proper folding to its native structure.[49] Given the sensitivity of NRVS to subtle changes in the CXXCH motif, this technique could potentially be used to probe structural changes of the heme (heme distortion) during formation of the HCCS−apoCyt *c* complex and heme insertion.

■ CONCLUSIONS

Nuclear resonance vibrational spectroscopy of ferric *Ht c*-552 can reveal subtle structural changes induced by mutation that influence vibrational dynamics sensitive to the CXXCH pentapeptide loop flexibility (250−325 cm^{-1}), the degree of heme distortion (380−400 cm^{-1}), and the strength of the Fe−N_{His} interaction (360−400 cm^{-1}). NRVS is therefore ideally suited for the elucidation of structural changes to the heme in Cyt *c* variants (as shown here) and upon complex formation with another protein, which will be the subject of future studies. Our results further indicate that the heme and CXXCH pentapeptide are strongly vibrationally coupled, and that the CXXCH loop is able to modulate the low-energy vibrations of the heme. This strong coupling is potentially significant for modulating electron transfer (ET). For example, binding of a redox partner to Cyt *c* could modulate the degree of heme ruffling and the vibrational dynamics of the heme *via the CXXCH loop*. This could potentially be used by the protein (a) to reduce the degree of heme ruffling to increase ET rates, (b) to modulate the heme vibrations and transfer thermal energy (transformed into vibrational energy via inelastic collision processes) to the heme to reach the transition state for ET, or (c) to adjust the directionality of the Fe−N_{pyrr} stretching vibration to direct the hole/electron to be transferred to pyrrole

DOI: 10.1021/bi501430z
Biochemistry 2015, 54, 1064−1076

II of the heme, which is in close contact to bound redox partners on the protein surface. With respect to point (b), the free energy released upon formation of the protein−protein complex of Cyt *c* with its redox partner could be transduced from the protein surface to the heme via vibrational excitation of the CXXCH loop. However, because formation of the protein−protein complex is usually slow, it is not clear how in this scenario, loss of the free energy into the solvent pool (in the form of heat) could be avoided, so this is probably the least likely possibility.

Given the sensitivity of NRVS to the seemingly subtle structural modifications studied herein, it is expected that perturbations such as protein−protein or protein−membrane interactions would also have a significant effect and could be detected and analyzed in terms of structural and dynamic alterations of the Cyt *c* active site via NRVS. Future work is directed toward elucidating the functional significance of the heme−polypeptide dynamic interactions for ET. NRVS is a key technique in this regard because of its incredible sensitivity toward minute changes in the active site environment that affect heme structure and vibrational dynamics.

■ ASSOCIATED CONTENT

Supporting Information

Experimental (Raman spectra) and theoretical (structure of the active site model, QCC-NCA refit of the NRVS data, force constants, and vibrational assignments) data for *Ht c*-552. This material is available free of charge via the Internet at http://pubs.acs.org.

■ AUTHOR INFORMATION

Corresponding Authors

*E-mail: mig11@psu.edu.
*E-mail: bren@chem.rochester.edu.
*E-mail: lehnertn@umich.edu.

Funding

K.L.B. acknowledges support from the National Institutes of Health (R01-GM63170).

Notes

The authors declare no competing financial interest.

■ ACKNOWLEDGMENTS

Use of the Advanced Photon Source is supported by the U.S. Department of Energy, Basic Energy Sciences, Office of Science, under Contract DE-AC02-06CH11357.

■ ADDITIONAL NOTE

[a]Interestingly, for both mutants that have Met13 substituted for Val, our QCC-NCA simulations suggest a minimal influence of the Met13 side chain itself on the NRVS data. However, because the methionine side chain is truncated in the current model, this might underplay its effect on the NRVS data. This cannot be further investigated without a very significant increase of the size of our computational model, which is not feasible for practical reasons.

■ REFERENCES

(1) Klinman, J. P., and Kohen, A. (2013) Hydrogen tunneling links protein dynamics to enzyme catalysis. *Annu. Rev. Biochem. 82*, 471−496.

(2) Barth, A. (2007) Infrared spectroscopy of proteins. *Biochim. Biophys. Acta 1767*, 1073−1101.

(3) Oladepo, S. A., Xiong, K., Hong, Z., Asher, S. A., Handen, J., and Lednev, I. K. (2012) UV resonance Raman investigations of peptide and protein structure and dynamics. *Chem. Rev. 112*, 2604−2628.

(4) Spiro, T. G. (1983) Iron Porphyrins. In *Iron Porphyrins* (Lever, A. B. P., and Gary, H. B., Eds.) pp 89−159, Addison-Wesley, Reading, MA.

(5) Spiro, T. G., and Czernuszewicz, R. S. (2000) In *Physical Methods in Bioinorganic Chemistry* (Que, L., Jr., Ed.) pp 59−120, University Science Books, Sausalito, CA.

(6) Zimmermann, J., Thielges, M. C., Yu, W., Dawson, P. E., and Romesberg, F. E. (2011) Carbon-deuterium bonds as site-specific and nonperturbative probes for time-resolved studies of protein dynamics and folding. *J. Phys. Chem. Lett. 2*, 412−416.

(7) Thielges, M. C., and Fayer, M. D. (2012) Protein dynamics studied with ultrafast two-dimensional infrared vibrational echo spectroscopy. *Acc. Chem. Res. 45*, 1866−1874.

(8) King, J. T., Arthur, E. J., Brooks, C. L. I., and Kubarych, K. J. (2014) Crowding induced collective hydration of biological macromolecules over extended distances. *J. Am. Chem. Soc. 136*, 188−194.

(9) Sturhahn, W. (2004) Nuclear resonant spectroscopy. *J. Phys.: Condens. Matter 16*, S497−S530.

(10) Sage, J. T., Paxson, C., Wyllie, G. R. A., Sturhahn, W., Durbin, S. M., Champion, P. M., Alp, E. E., and Scheidt, W. R. (2001) Nuclear resonance vibrational spectroscopy of a protein active-site mimic. *J. Phys.: Condens. Matter 13*, 7707−7722.

(11) Rai, B. K., Durbin, S. M., Prohofsky, E. W., Sage, J. T., Wyllie, G. R. A., Scheidt, W. R., Sturhahn, W., and Alp, E. E. (2002) Iron normal mode dynamics in (nitrosyl)iron(II)tetraphenylporphyrin from X-ray nuclear resonance data. *Biophys. J. 82*, 2951−2963.

(12) Rai, B. K., Durbin, S. M., Prohofsky, E. W., Sage, J. T., Ellison, M. K., Roth, A., Scheidt, W. R., Sturhahn, W., and Alp, E. E. (2003) Direct determination of the complete set of iron normal modes in a porphyrin-imidazole model for carbonmonoxy-heme proteins: [Fe(TPP)(CO)(1-MeIm)]. *J. Am. Chem. Soc. 125*, 6927−6936.

(13) Scheidt, W. R., Durbin, S. M., and Sage, J. T. (2005) Nuclear resonance vibrational spectroscopy: NRVS. *J. Inorg. Biochem. 99*, 60−71.

(14) Lehnert, N., Galinato, M. G. I., Paulat, F., Richter-Addo, G. B., Sturhahn, W., Xu, N., and Zhao, J. (2010) Nuclear resonance vibrational spectroscopy applied to [Fe(OEP)(NO)]: The vibrational assignments of five-coordinate ferrous heme-nitrosyls and implications for electronic structure. *Inorg. Chem. 49*, 4133−4148.

(15) Lehnert, N., Sage, J. T., Silvernail, N., Scheidt, W. R., Alp, E. E., Sturhahn, W., and Zhao, J. (2010) Oriented single-crystal nuclear resonance vibrational spectroscopy of [Fe(TPP)(MI)(NO)]: Quantitative assessment of the *trans* effect of NO. *Inorg. Chem. 49*, 7197−7215.

(16) Lehnert, N. (2009) Quantum Chemistry Centered Normal Coordinate Analysis (QCC-NCA): Routine Application of Normal Coordinate Analysis for the Simulation of the Vibrational Spectra of large Molecules. In *Computational Inorganic and Bioinorganic Chemistry* (Solomon, E. I., King, R. B., and Scott, R. A., Eds.) pp 123−140, John Wiley & Sons, Chichester, U.K.

(17) Galinato, M. G. I., Kleingardner, J. G., Bowman, S. E. J., Alp, E. E., Zhao, J., Bren, K. L., and Lehnert, N. (2012) Heme-protein vibrational couplings in cytochrome *c* provide a dynamic link that connects the heme-iron and the protein surface. *Proc. Natl. Acad. Sci. U.S.A. 109*, 8896−8900.

(18) Bowman, S. E. J., and Bren, K. L. (2008) The chemistry and biochemistry of heme *c*: Functional bases for covalent attachment. *Nat. Prod. Rep. 25*, 1118−1130.

(19) Liu, X. S., Kim, C. N., Yang, J., Jemmerson, R., and Wang, X. D. (1996) Induction of apoptotic program in cell-free extracts: Requirement for dATP and cytochrome *c*. *Cell 86*, 147−157.

(20) Zhao, Y. G., Wang, Z. B., and Xu, J. X. (2003) Effect of cytochrome *c* on the generation and elimination of O formula and H_2O_2 in mitochondria. *J. Biol. Chem. 278*, 2356−2360.

DOI: 10.1021/bi501430z
Biochemistry 2015, 54, 1064−1076

(21) Liptak, M. D., Wen, X., and Bren, K. L. (2010) NMR and DFT investigation of heme ruffling: Functional implications for cytochrome *c*. *J. Am. Chem. Soc. 132*, 9753−9763.
(22) Michel, L. V., Ye, T., Bowman, S. E. J., Levin, B. D., Hahn, M. A., Russell, B. S., Elliott, S. J., and Bren, K. L. (2007) Heme attachment motif mobility tunes cytochrome c redox potential. *Biochemistry 46*, 11753−11760.
(23) Bowman, S. E. J., and Bren, K. L. (2010) Variation and Analysis of Second-Sphere Interactions and Axial Histidinate Character in c-type Cytochromes. *Inorg. Chem. 49*, 7890−7897.
(24) Can, M., Zoppellaro, G., Andersson, K. K., and Bren, K. L. (2011) Modulation of ligand-field parameters by heme ruffling in cytochromes c revealed by EPR spectroscopy. *Inorg. Chem. 50*, 12018−12024.
(25) Becke, A. D. (1988) Density-functional exchange-energy approximation with correct asymptotic behavior. *Phys. Rev. A 38*, 3098−3100.
(26) Perdew, J. P. (1986) Density-functional approximation for the correlation-energy of the inhomogeneous electron-gas. *Phys. Rev. B: Condens. Matter Mater. Phys. 33*, 8822−8824.
(27) Wadt, W. R., and Hay, P. J. (1985) Ab initio effective core potentials for molecular calculations. Potentials for the transition metal atoms Sc to Hg. *J. Chem. Phys. 82*, 270−283.
(28) Wadt, W. R., and Hay, P. J. (1985) Ab initio effective core potentials for molecular calculations. Potentials for main group elements Na to Bi. *J. Chem. Phys. 82*, 284−298.
(29) Wadt, W. R., and Hay, P. J. (1985) Ab initio effective core potentials for molecular calculations. Potentials for K to Au including the outermost core orbitals. *J. Chem. Phys. 82*, 299−311.
(30) Praneeth, V. K. K., Näther, C., Peters, G., and Lehnert, N. (2006) Spectroscopic Properties and Electronic Structure of Five- and Six-Coordinate Iron(II) Porphyrin NO Complexes: Effect of the Axial N-Donor Ligand. *Inorg. Chem. 45*, 2795−2811.
(31) Paulat, F., Berto, T. C., DeBeer George, S., Goodrich, L. E., Praneeth, V. K. K., Sulok, C. D., and Lehnert, N. (2008) Vibrational assignments of six-coordinate ferrous heme nitrosyls: New insight from nuclear resonance vibrational spectroscopy. *Inorg. Chem. 47*, 11449−11451.
(32) Spiro, T. G., and Li, X.-Y. (1988) *Resonance Raman Spectra of Heme and Metalloproteins*, Wiley, New York.
(33) Strekas, T. C., and Spiro, T. G. (1972) Cytochrome *c*: Resonance Raman spectra. *Biochim. Biophys. Acta 278*, 188−192.
(34) Hu, S., Morris, I. K., Singh, J. P., Smith, K. M., and Spiro, T. G. (1993) Complete assignment of cytochrome c resonance Raman spectra via enzymatic reconstitution with isotopically labeled hemes. *J. Am. Chem. Soc. 115*, 12446−12458.
(35) Paulat, F., Praneeth, V. K. K., Näther, C., and Lehnert, N. (2006) Quantum Chemistry-Based Analysis of the Vibrational Spectra of Five-Coordinate Metalloporphyrins [M(TPP)Cl]. *Inorg. Chem. 45*, 2835−2856.
(36) Franzen, S., Boxer, S. G., Dyer, B., and Woodruff, W. H. (2000) Resonance Raman studies of heme axial ligation in H93G myoglobin. *J. Phys. Chem. B 104*, 10359−10367.
(37) Leu, B. M., Ching, T. H., Zhao, J., Sturhahn, W., Alp, E. E., and Sage, J. T. (2009) Vibrational dynamics of iron in cytochrome c. *J. Phys. Chem. B 113*, 2193−2200.
(38) Travaglini-Allocatelli, C., Gianni, S., Dubey, V. K., Borgia, A., Di Matteo, A., Bonivento, D., Cutruzzolà, F., Bren, K. L., and Brunori, M. (2005) An obligatory intermediate in the folding pathway of cytochrome c-552 from *Hydrogenobacter thermophilus*. *J. Biol. Chem. 280*, 25729−25734.
(39) Johannessen, C., White, P. C., and Abdali, S. (2007) Resonance Raman optical activity and surface enhanced resonance Raman optical activity analysis of cytochrome c. *J. Phys. Chem. A 111*, 7771−7776.
(40) Berthomieu, C., Marboutin, L., Dupeyrat, F., and Bouyer, P. (2006) Electrochemically induced FTIR difference spectroscopy in the mid- to far infrared (200 mm) domain: A new setup for the analysis of metal-ligand interactions in redox proteins. *Biopolymers 82*, 363−367.
(41) Ma, J. G., Laberge, M., Song, X. Z., Jentzen, W., Jia, S. L., Zhang, J., Vanderkooi, J. M., and Shelnutt, J. A. (1998) Protein-induced changes in nonplanarity of the porphyrin in nickel cytochrome *c* probed by resonance Raman spectroscopy. *Biochemistry 37*, 5118−5128.
(42) Matsuura, Y., Takano, T., and Dickerson, R. E. (1982) Structure of Cytochrome c_{551} from *Pseudomonas aeruginosa* refined at 1.6 Å resolution and comparison of the two redox forms. *J. Mol. Biol. 156*, 389−409.
(43) La Mar, G. N., de Ropp, J. S., Chacko, V. P., Satterlee, J. D., and Erman, J. E. (1982) Axial histidyl imidazole non-exchangeable proton resonances as indicators of imidazole hydrogen-bonding in ferric cyanide complexes of heme peroxidases. *Biochim. Biophys. Acta 708*, 317−325.
(44) O'Brien, P., and Sweigart, D. A. (1985) Effect of redox potentials of hydrogen bonding from coordinated imidazole in metalloporphyrin complexes. *Inorg. Chem. 24*, 1405−1409.
(45) Quinn, R., Mercer-Smith, J., Bursyn, J. N., and Valentine, J. S. (1984) Influence of hydrogen bonding on the properties of iron porphyrin imidazole complexes: An internally hydrogen-bonded imidazole ligand. *J. Am. Chem. Soc. 106*, 4136−4144.
(46) Marcus, R. A., and Sutin, N. (1985) Electron transfers in chemistry and biology. *Biochim. Biophys. Acta 811*, 265−322.
(47) Bertini, I., Cavallaro, G., and Rosato, A. (2011) Principles and patterns in the interaction between mono-heme cytochrome *c* and its partners in electron transfer processes. *Metallomics 3*, 354−362.
(48) Zhang, Y., Stevens, J. M., and Ferguson, S. J. (2014) Substrate recognition of holocytochrome *c* synthase: N-terminal region and CXXCH motif of mitochondrial cytochrome *c*. *FEBS Lett. 588*, 3367−3374.
(49) Babbitt, S. E., San Francisco, B., Mendez, D. L., Lukat-Rodgers, G. S., Rodgers, K. R., Bretsnyder, E. C., and Kranz, R. G. (2014) Mechanisms of mitochondrial holocytochrome *c* synthase and the key roles played by cysteins and histidine of the heme attachment site, CysXXCysHis. *J. Biol. Chem. 289*, 28795−28807.
(50) Simeonov, M., Altuve, A., Massiah, M. A., Wang, A., Eastman, M. A., Benson, D. R., and Rivera, M. (2005) Mitochondrial and microsomal ferric *b*-5 cytochromes exhibit divergent conformational plasticity in the context of a common fold. *Biochemistry 44*, 9308−9319.
(51) Hobbs, J. D., and Shelnutt, J. A. (1995) Conserved nonplanar heme distortions in cytochromes c. *J. Protein Chem. 14*, 19−25.
(52) Ma, J. G., Vanderkooi, J. M., Zhang, J., Jia, S. L., and Shelnutt, J. A. (1999) Resonance Raman investigation of nickel microperoxidase-11. *Biochemistry 38*, 2787−2795.
(53) Jentzen, W., Ma, J. G., and Shelnutt, J. A. (1998) Conservation of the conformation of the porphyrin macrocycle in hemoproteins. *Biophys. J. 74*, 753−763.
(54) Borgia, A., Bonivento, D., Travaglini-Allocatelli, C., Di Matteo, A., and Brunori, M. (2006) Unveling the hidden folding intermediate in c-type cytochromes by protein engineering. *J. Biol. Chem. 281*, 9331−9336.
(55) Sun, Y., Benabbas, A., Zeng, W., Kleingardner, J. G., Bren, K. L., and Champion, P. M. (2014) Investigations of heme distortion, low-frequency vibrational excitations, and electron transfer in cytochrome c. *Proc. Natl. Acad. Sci. U.S.A. 111*, 6570−6575.
(56) Berezhna, S., Wohlrab, H., and Champion, P. M. (2003) Resonance Raman investigation of cytochrome c conformational change upon interaction with membranes of intact and Ca^{2+}-exposed mitochondria. *Biochemistry 42*, 6149−6158.

DOI: 10.1021/bi501430z
Biochemistry 2015, 54, 1064−1076